Solid State Communications 252 (2017) 22–28

Contents lists available at ScienceDirect

Solid State Communications

journal homepage: www.elsevier.com/locate/ssc

Communication

MgF_2 monolayer as an anti-reflecting material

H.R. Mahida[a], Deobrat Singh[b], Yogesh Sonvane[b,*], Sanjeev K. Gupta[c,*], P.B. Thakor[a]

[a] Department of Physics, Veer Narmad South Gujarat University, Surat 395007, India
[b] Advanced Material Lab, Department of Applied Physics, S. V. National Institute of Technology, Surat 395007, India
[c] Computational Materials and Nanoscience Group, Department of Physics and Electronics, St. Xavier's College, Ahmedabad 380009, India

ARTICLE INFO

Keywords:
2D Monolayer
Ab-initio approach
Electronic properties
Optical properties

ABSTRACT

The single-layer atomic sheet of magnesium fluoride (MgF_2) having 1H and 1T phase structure (hexagonal and tetragonal phase) has been calculated by density functional theory (DFT). Further, we have investigated the structural, electronic and optical properties such as frequency dependent dielectric function, absorption spectra, energy loss spectra, reflectivity, refractive index and optical conductivity of monolayer MgF_2 for the direction of parallel and perpendicular electric field polarizations. Our results suggest that monolayer MgF_2 provides promising applications in anti-reflection coatings, high-reflective systems and in opto-electronic materials.

1. Introduction

Magnesium fluoride (MgF_2) material has unique optical property which remains transparent over an extremely wide range of photon energies. Magnesium fluoride (MgF_2) has increased in popularity to become the ideal anti-reflection coating for laser devices, the important material in optical fibre communication and the potential item in luminescent, due to its wide band gap, low refractive index, excellent mechanical properties and high laser damage resistance [1–3]. It is one of the two-dimensional (2D) materials that transmit in the vacuum ultraviolet region and finds its applications in optical windows, lenses, and prisms etc. [1–6]. Further, halide group fluoride based semiconductors have received considerable interest because they are known as the third generation of semi-conductor and insulator materials in the microelectronics industry. It is of great importance due to its optoelectronic properties, high thermal and mechanical stability as similar to GaN material [7]. Nowadays, it is already used in blue and ultraviolet light emitting diodes (LEDs) and room-temperature laser diodes with long operating lifetimes [8,9]. Fluorides such as MgF_2 are typical materials to make optical coatings for laser applications in the ultraviolet UV spectral region [10,11]. Magnesium fluoride has been used in MgF_2-doped chromium or aluminium fluoride catalysts for exchange on hydrochlorocarbons [12]. The magnesium fluoride solution is used for anti-reflective coatings on glass substrates and properties can be tuned by changing the viscosity, particle size distribution and structural parameters [13]. It is clear that the use of magnesium fluoride as a support for different catalytic materials, transition metal oxides like MoO_3, V_2O_5, WO_3 [14,15] and binary systems such as CuO and Cr_2O_3 [13,16,17] more over for metallic catalysts like ruthenium ones [13,17–20] is appealing. In past the theoretical study of rutile structure of MgF_2 reports that it is important radiation-resistant material with numerous applications due to its transparency from vacuum ultraviolet to infrared range of photon energies [21–24]. In this paper, we have studied 2D- thick layer of magnesium fluoride and determine the structural, electronic, dielectric function and the optical band gap using DFT. The structural, electronic and optical properties of MgF_2 monolayer are presented and discussed in comparison with the available theoretical results in Section 3 while methodology is discussed in Section 2.

2. Methodology

We have used first principles calculation based on DFT to obtained the band structure of bulk tetragonal, 2D monolayer of 1H and 1T phase of magnesium difluoride (MgF_2) system. These were performed using the Vienna Ab-initio Simulation Package (VASP) [25,26]. The core electrons were treated using the projector-augmented-wave method for the self-consistent total energy calculations and geometry optimization. We have used the generalized gradient approximation (GGA) given by Perdew-Burke-Ernzerhof (PBE) functional for exchange- correlation potential [27–29]. The electronic structure calculations, the random-phase approximation (RPA) to the correlation energy are supposed to be a suitable complement to the exact exchange energy [30]. The kinetic energy cut-off for the plane wave basic set is taken to be 400 eV. The Brillouin-zone (BZ) integration was sampled by 11×11×11 and 11×11×1 k-grid mesh for bulk tetragonal, 1H and 1T phase of MgF_2 respectively. The convergence criteria for energy in SCF (self consistent field) cycles are chosen to be 10^{-6} eV. The material is

* Corresponding authors.
E-mail addresses: yas@phy.svnit.ac.in (Y. Sonvane), sanjeev.gupta@sxca.edu.in (S.K. Gupta).

http://dx.doi.org/10.1016/j.ssc.2017.01.005
Received 28 September 2016; Received in revised form 8 December 2016; Accepted 7 January 2017
Available online 08 January 2017

periodic in XY-plane and to prevent the interaction between adjacent layers are more than 18 Å vacuum spacing is kept in Z-direction for 1H and 1T phase of MgF_2.

The frequency dependent complex dielectric function $\varepsilon(\omega) = \varepsilon_1(\omega) + i\varepsilon_2(\omega)$ is known to describe the optical properties of materials, where ε_1 and ε_2 are the real and imaginary components in polarization direction of the dielectric functions [7,31], respectively.

$$\varepsilon_1(\omega) = 1 + \frac{2}{\pi} p \int_0^{\infty} \frac{\omega' \varepsilon_2(\omega') d\omega'}{(\omega'^2 - \omega^2)} \tag{1}$$

$$\varepsilon_2(\omega) = \left(\frac{4\pi^2 e^2}{m^2 \omega^2}\right) \sum_{i,j} \int_k \langle i\, Mj \rangle^2 f_i (1 - f_i) \times \delta(E_{j,k} - E_{i,k} - \omega) d^3k \tag{2}$$

The reflectivity, reflective index, energy loss spectrum, optical conductivity and Absorption coefficient are calculated from the following relation,

$$R(\omega) = \left| \frac{\sqrt{\varepsilon(\omega)} - 1}{\sqrt{\varepsilon(\omega)} + 1} \right|^2 \tag{3}$$

$$n(\omega) = \left[\frac{\sqrt{\varepsilon_1(\omega)^2 + \varepsilon_2(\omega)^2}}{2} + \frac{\varepsilon_1(\omega)}{2} \right]^{1/2} \tag{4}$$

$$L(\omega) = \frac{\varepsilon_2(\omega)}{\varepsilon_1(\omega)^2 + \varepsilon_2(\omega)^2} \tag{5}$$

$$\sigma(\omega) = \frac{\omega}{4\pi} \varepsilon_2(\omega) \tag{6}$$

$$\alpha(\omega) = \sqrt{2}\,(\omega)[\varepsilon(\omega) - \varepsilon_1(\omega)]^{1/2} \tag{7}$$

Here, $\varepsilon(\omega) = \sqrt{\varepsilon_1(\omega)^2 + \varepsilon_2(\omega)^2}$ is the relative dielectric constant.

3. Results and discussions

3.1. Optimised structure

The optimised structure of bulk tetragonal MgF_2 is depicted in the Fig. 1. The optimised bond length of MgF_2 bulk is 1.98 Å between Mg-F atom. We obtained optimised lattice constant a=4.62 Å and c/a=0.66 for bulk MgF_2 [32]. The calculated cohesive energy of bulk MgF_2 is 15.30 eV [33].

The relaxed 1H and 1T phase crystal structure and unit cell of MgF_2 monolayer as shown in the Fig. 2. The optimised bond lengths of both phases 1H and 1T-MgF_2 are 2.66 Å and 2.84 Å between F-F elements and 2.18 Å and 2.02 Å between Mg-F elements and angle between F-Mg-F is 74.98° and 89.15°, respectively. We obtained optimised lattice constant a=2.83 Å and 2.88 Å and c/a=4.03 and 6.74 for 1H and 1T phase, respectively. It is clear that the calculated equilibrium lattice constant a_0 is 2.83 Å (1H) and 2.88 Å (1T). The calculated cohesive energy of 1H and 1T phases of MgF_2 are 14.25 eV and 15.07 eV.

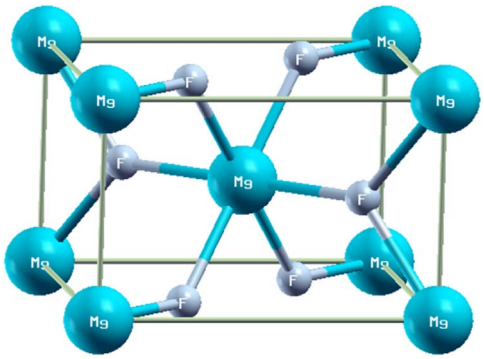

Fig. 1. The optimised structure of bulk tetragonal MgF_2.

3.2. Band structure and density of states

The calculated electronic band structure along the high-symmetry directions in the first Brilluin zone (BZ) of the bulk tetragonal MgF_2 structure is shown in Fig. 3(a). The energy band-gap E_g is 7.07 eV at high symmetry point Γ for bulk tetragonal MgF_2 structure. Therefore, bulk tetragonal MgF_2 is direct band-gap with wide band-gap material (pure insulator). The theoretical value of the band gap of the bulk was 6.84 eV, much smaller than the experimental result of 10.8 eV [34] which is good agrement with previous reported work in ref. [11]. There are some other measured band gaps of bulk MgF_2 from experiments ranges from 10.8eV to 12.4 eV [35–37].

It is well known that the calculated band gaps are underestimated from the nature of the electronic band structure as DFT underestimate the band gaps [35–37]. We have also calculated the total density of states (TDOS) and partial density of states (PDOS) of Mg, F and MgF_2 as shown in Fig. 3(b). The contribution of F atom in the electronic levels are more dominant as compared to Mg atom. In case of lower side of density of states, the contribution of electronic levels is higher in the range of −21.10 eV to −19.71 eV. The F atoms are highly localized in general and easily identified as sharp peaks in the total DOS near the Fermi level and highly localized. The conduction band is extensive and spill over a spacious range of energies.

The computed electronic energy band structure along the high-symmetry directions in the first Brillouin zone (BZ) of 1H and 1T MgF_2 structure is shown in the Fig. 4(a–b). The 1H and 1T phases of monolayer MgF_2 has a conduction band minimum (CBM) at the Γ-point and valence band maximum (VBM) at the Γ point both have same value of k-points show it is direct band gap. The energy band-gap width E_g is 6.16 eV and 7.56 eV at high symmetry point Γ for 1H and 1T phases of MgF_2 structure. Thus, both the phases 1H and 1T of MgF_2 are direct energy band-gap in monolayer. The theoretical value of the band gap of the bulk was 6.84 eV, much smaller than the experimental result of 10.8 eV. The energy band-gap in case of monolayer 1H and 1T monolayer is found 6.16 eV and 7.56 eV in 2D monolayer, which is a lie between theoretical value and experimental value [34]. Some other measured band gaps of bulk MgF_2 from experiments range from 10.8 to 12.4 eV [35–37]. The direct band gap, 6.78 eV obtained from the DFT-GGA calculation, is much smaller than the experimental value. We have also calculated the total density of states (TDOS) and partial density of states of Mg, F and MgF_2 as shown in Fig. 4(c) and (d).

The contribution of F atom the electronic levels are more dominant as compared to Mg atom. In case of lower side of density of states, the contribution of electronic levels is higher in the range of −21.87 eV to −19.10 eV. The F atoms are highly localized in general and easily identified as sharp peaks in the total DOS near the Fermi levels of F-atom similar to the bulk nature of MgF_2. Fig. 4(d) represents the total and partial density of states of 1T-MgF_2. The contribution of F atom the electronic level is more dominant as compare to Mg atom. And the lower side of density of states, the contribution of electronic levels is higher in the range of −20.12 eV to −19.06 eV. It can be seen in Fig. 4(d) that F atoms are easily indicate sharp peaks in the total DOS near the Fermi levels and highly localized.

3.3. Optical properties

The calculated parallel and perpendicular component of imaginary part of the frequency dependent complex dialectic function Im ε(ω) as shown in the Fig. 5 (1H and 1T phases). The imaginary part Im ε(ω) is directly related to the electronic band structure of a material and can be described by absorptive behaviour as shown in Fig. 4(a-b). It show that the imaginary parts of dielectric function by considering inter-band transitions for both directions of electric field i.e. the electric field polarized parallel to the MgF_2 monolayer (E||X), and perpendicular to the MgF_2 monolayer (E⊥Z). The spectra of MgF_2 monolayer consists of a many distinct peaks that can be traced to dipole-allowed transition

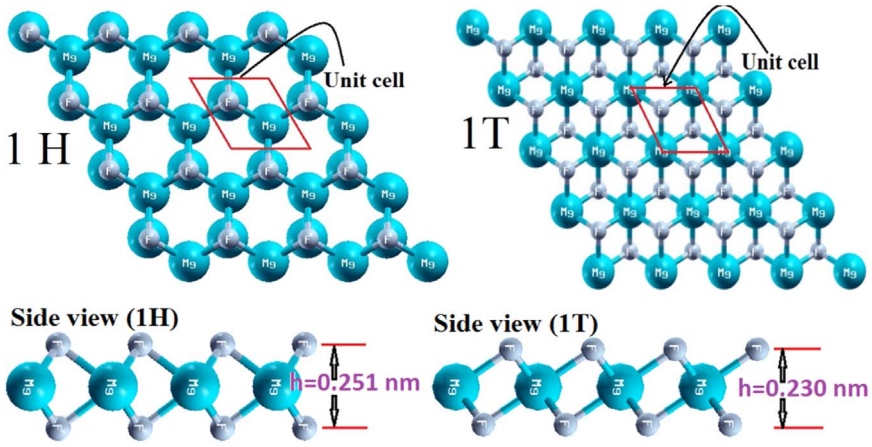

Fig. 2. The optimised structure of 1H and 1T phases of MgF_2 structure monolayer with top view and side view.

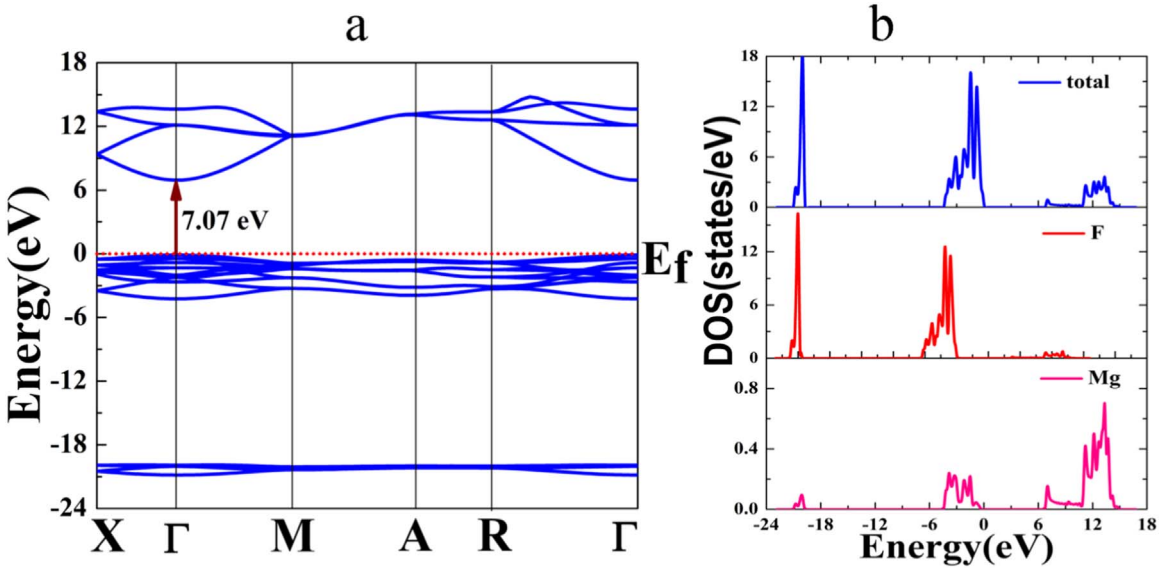

Fig. 3. (a) The Electronic band structure of bulk tetragonal MgF_2, and the zero energy is set to the Fermi energy (level) and (b) It is represented as total partial density of state (PDOS) of bulk tetragonal MgF_2.

between states near the Van Hove singularities (VHS) [38,39]. It is clearly seen from Fig. 5 that dielectric function of MgF_2 monolayer depends on the direction of polarization of light. These peaks arise in the range of 5.85–31.22 eV (1H-phase) and of 7.71–31.44 eV (1H-phase) in both cases parallel and perpendicular component of imaginary dielectric function respectively. The threshold energy of the dielectric function occurs at E_0 =6.16 eV (1T-phase) and 7.56 eV (1T-phase), which correspond to the fundamental gap at equilibrium. It is well known that materials with band gaps larger than 4 eV in the ultraviolet region [40,41] indicate that MgF_2 will work excellently in the UV region as an optical material.

3.3.1. Refractive index

The calculated refraction index of 1H and 1T-MgF_2 phases is shown in Fig. 6 (1H and1T phase). The value of static refractive index for electric field parallel to 1H and 1T-MgF_2 monolayer is 1.37, 1.375 and the electric field perpendicular to MgF_2 monolayer is 1.39, 1.33 respectively. The experimental result for the bulk MgF_2 crystal structure has been taken, the refractive index is 1.34 but in work we found 1.37 (1H-phase) and 1.33 (1T-phase) perpendicular to the monolayer. The refractive index is 1.39 (1H-phase) and 1.375 (1T-phase) parallel components to the monolayer. These results are very close to the experimental value [12,39,40]. The lower refractive index of the MgF_2 ultra-thin nano-films confirms that the material has promising applications in anti-reflection coatings and high-reflective systems.

3.3.2. Absorption coefficient

The optical absorption coefficient α(ω) of 1H and 1T-MgF_2 is shown in the Fig. 7(1H and 1T phase). The optical absorption energy (E_{op}) could be obtained from the following relation,

$$\alpha h\upsilon = A(h\upsilon - E_{op})^n \quad (8)$$

Where hυ is the photon energy, A is a constant, and α is the optical absorption coefficient. We used n =2 for a direct band-gap material. Using the linear extrapolation method, the direct absorption curve with phonon absorption ($E_{g(dir)} - E_{ph}$) is determined to 5.32 eV, where $E_{g(dir)}$ is the direct band gap and E_{ph} is the phonon energy for 1H-phase. This shows that the absorption curve starts from about 5.32 eV, after which the intensity varies with the increase in photon energy, and reaches a maximum value of 13.53×10^5 cm^{-1} at 10.91 eV and 18.4×10^5 cm^{-1} at 18.61 eV for 1H-phase, parallel and perpendicular component respectively. There is no electronic transition in the lower energy range (E < 5.32 eV) because the energy of the photon is lower than the band gap of the material. The first peak in the absorption spectrum occurs at 7.06 eV and 8.98 eV for parallel and perpendicular component respectively, and other peaks occur at 9.63 eV, 10.91 eV, 15.40 eV, 18.61 eV and 20.53 eV, 22.46 eV, 26.31 eV for parallel

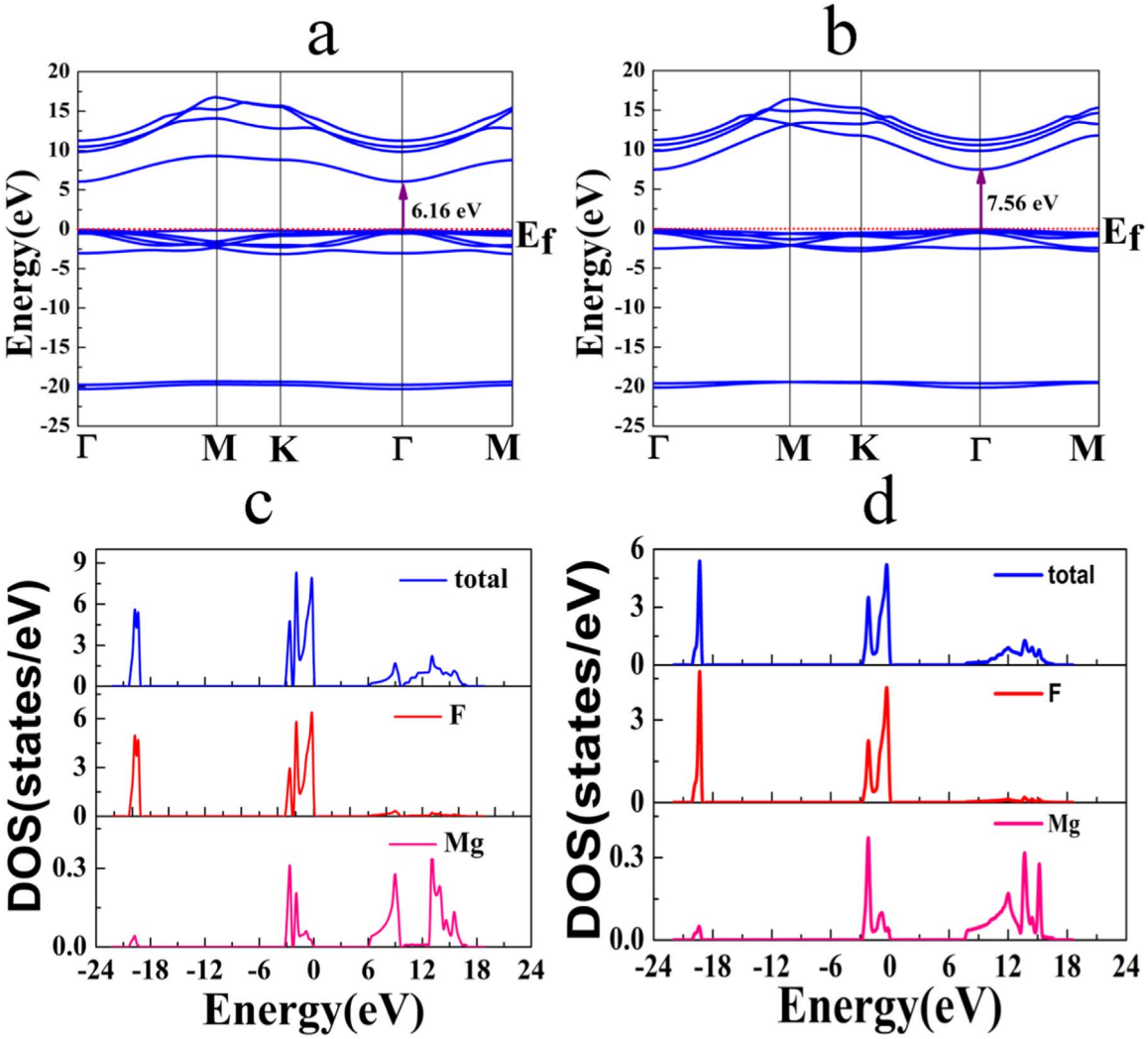

Fig. 4. The electronic band structure of 1H (a) and 1T (b) phases of MgF_2 monolayer. The zero energy is set to the Fermi energy (level) and the calculated total density of state of 1H (c) and 1T (d) phases of MgF_2 monolayer.

component and 10.91 eV, 13.48 eV, 18.61 eV, 19.89 eV, 23.74 eV, and 26.31 eV, for perpendicular component of 1H-phase of MgF_2 [42].

For 1T-phase of MgF_2, the direct absorption curve with phonon absorption ($Eg_{(dir)} - E_{ph}$) is determined to 7 eV, where $E_{g(dir)}$ is the direct band gap and E_{ph} is the phonon energy. This shows that the absorption curve starts from about 7 eV, after which the intensity varies with the increase in photon energy, and reaches a maximum value of 14.77×10^5 at 17.33 eV and 15.33×10^5 at 14.76 eV for parallel and perpendicular component respectively. There is no electronic transition in the low energy range ($E < 7$ eV) because the energy of

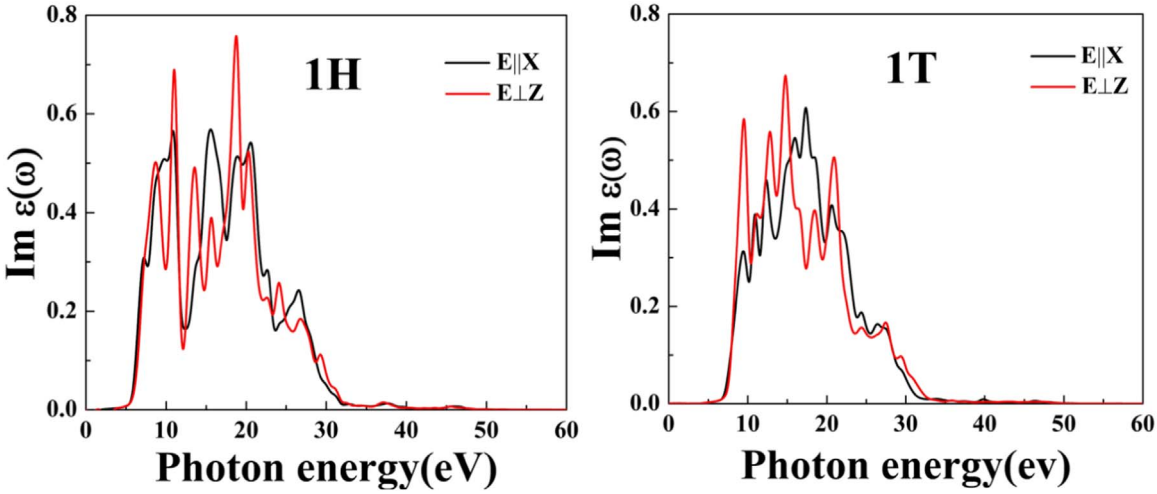

Fig. 5. Frequency dependent imaginary part of complex dielectric functions of 1 H and 1T-MgF_2 phase of monolayer.

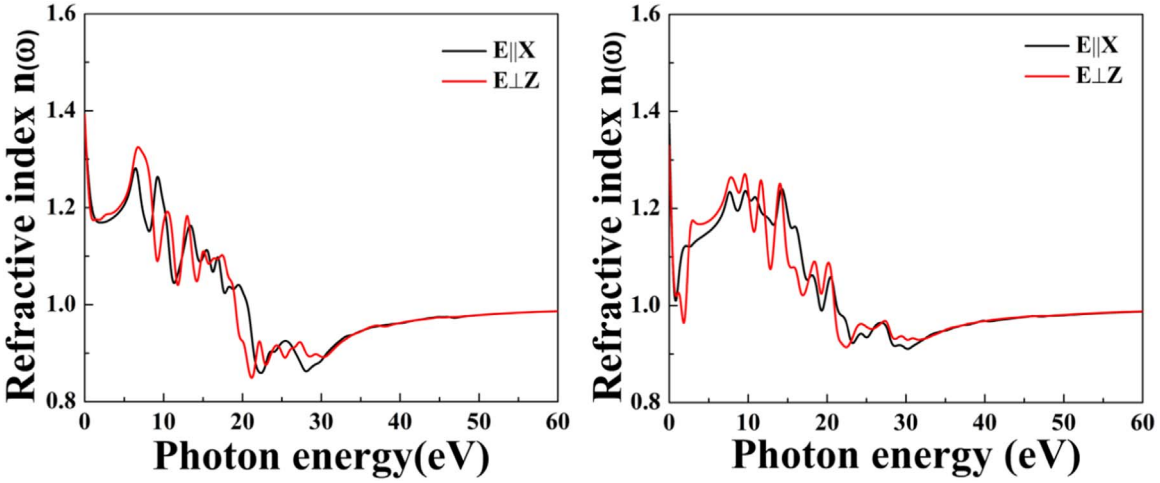

Fig. 6. 1H and 1T-MgF_2 phase represented the static refractive index of MgF_2 monolayer resolved different polarization direction.

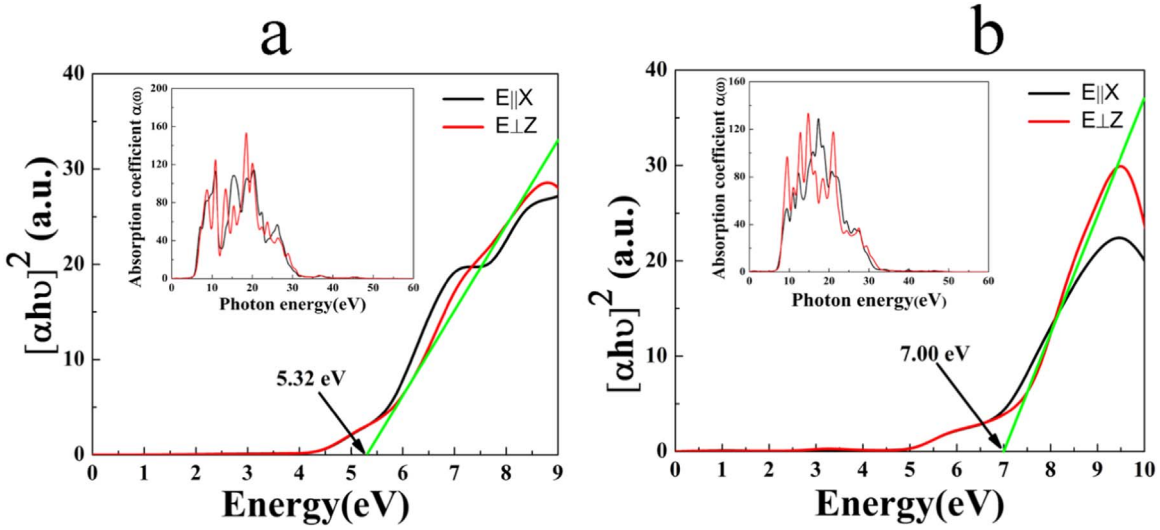

Fig. 7. The calculated optical absorption coefficient and variation of $(\alpha E)^2$ as a function of photon energy for 1 H and 1T-MgF_2 monolayer.

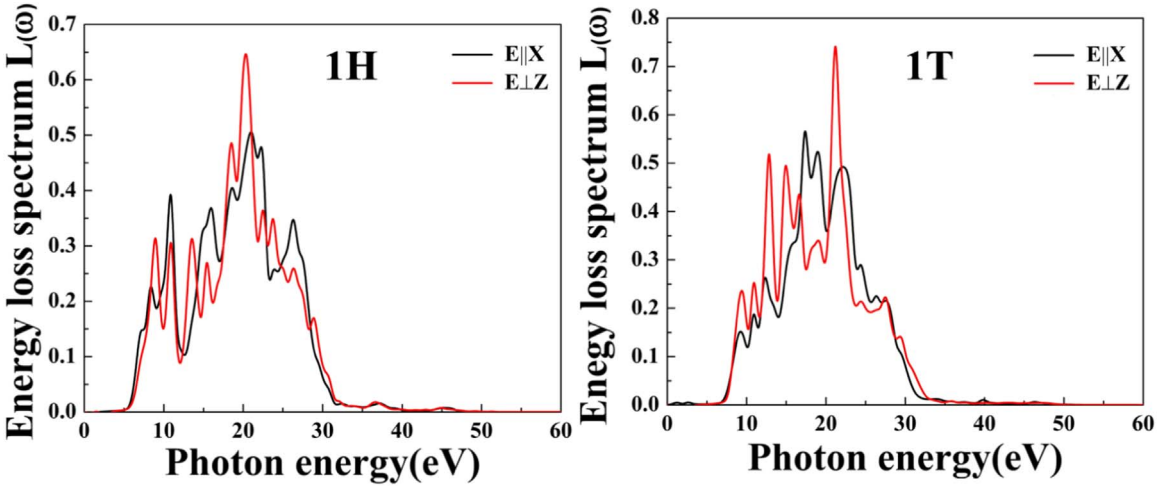

Fig. 8. Energy loss spectrum under parallel and perpendicular polarizations for 1H and 1T-MgF_2 monolayer.

the photon is lower than the band gap of the material. The first peak in the absorption spectrum occurs at 9.63 eV for both parallel and perpendicular component, and other peaks occur at16.04 eV, 18.61 eV, 20.53 eV, 24.38 eV and 26.31 eV for parallel component and 10.91 eV, 12.83 eV, 14.76 eV, 16.68 eV, 18.61 eV, 21.18 eV, and 24.38 eV for perpendicular component of 1T-MgF_2 [42].

3.3.3. Energy loss spectrum

The calculated energy loss spectrum L(ω) of 1H and 1T-phase of MgF_2 is represented in Fig. 8(1H) and (1T) . The loss function L(ω)

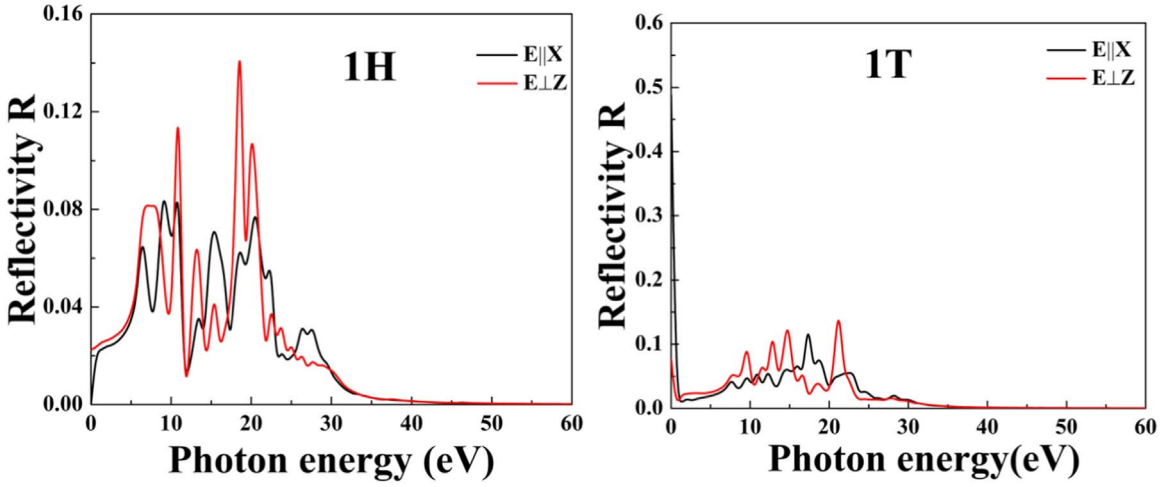

Fig. 9. Reflectivity of 1H and 1T-MgF_2 monolayer parallel and perpendicular polarizations.

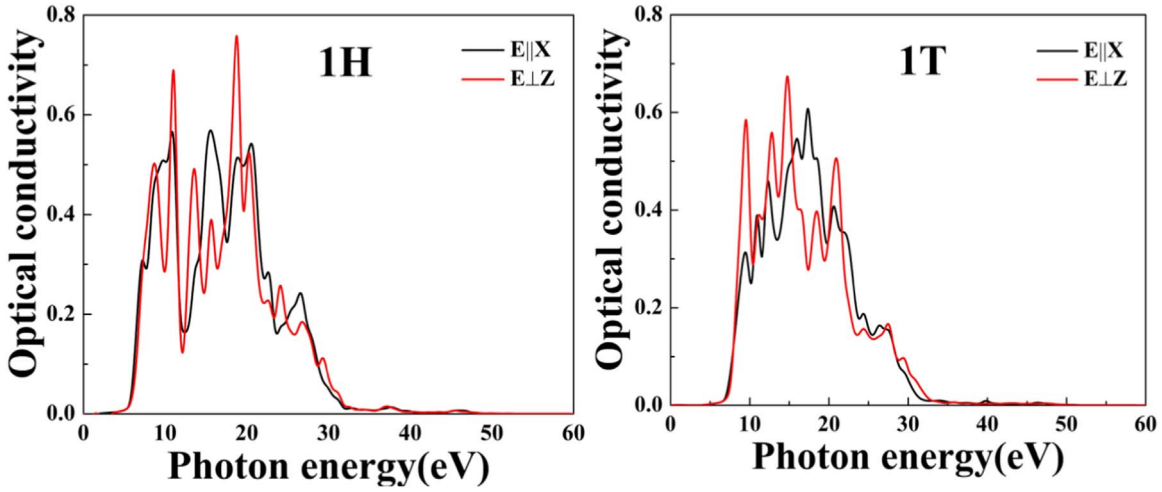

Fig. 10. The real part of optical conductivity corresponding to the imaginary part of the dielectric function.

which is also an important optical parameter describing the energy loss of a first electron travelling in the material. The peak of the loss spectrum represents the characteristic associated with plasma oscillation. Energy loss spectrum for 1H-MgF_2 monolayer in both directions of electric field is shown in Fig. 8 (1H). For the electric field parallel to the 1H- MgF_2 monolayer, there is a large broad resonance near the 20 eV. For (E||X), the energy loss function consists of more separated peaks. For (E⊥Z), the energy loss function consists of more separated peaks below the 19 eV. There is also a relatively broad resonance at around 20 eV and there is no distinct peak at energies above 20 eV for (E⊥Z). It shows that the resonant energy loss occurs at 22.46 eV and 20.53 eV for parallel and perpendicular direction. In case of 1T-phase of MgF_2, the energy loss spectrum in both directions of electric field is shown in Fig. 8 (1T). For the electric field parallel to the 1T-MgF_2 monolayer, there is a large broad resonance near 20 eV. For (E||X), the energy loss function consists of more separated peaks. For (E⊥Z), the energy loss function consists of more separated peaks below the 20 eV. There is also a relatively broad resonance at around 20 eV and there is no distinct peak at energies above 20 eV for (E⊥Z). Fig. 8(1T) shows that the resonant energy loss occurs at 17.33 eV and 21.18 eV for parallel and perpendicular direction.

3.3.4. Reflectivity

The reflectivity for 1H and 1T-MgF_2 monolayer for both the directions of electric field is shown in Fig. 9. In the low energy region for 1H-MgF_2 (below approximately 8.34 eV) (R||X) is higher than (R⊥Z), mainly owing to the stronger optical excitations in the (E||X) case. Whereas in the electric field perpendicular to of 1H MgF_2 monolayer, reflectivity at energy range between 8.98 eV and 22.46 eV is more. In the case of 1T-phase of MgF_2 monolayer, the low energy region (below approximately 8.98 eV) (R||X) is higher than (R⊥Z), mainly owing to the stronger optical excitations in the (E||X) case, while in the electric field perpendicular to 1T-MgF_2 monolayer, reflectivity at energy range between 9.62 eV and 23.10 eV is more. It is also found that in electric field parallel to 1H and 1T-MgF_2 monolayer, reflectivity at lower energy is more and at this energy range, transition is less.

3.3.5. Optical conductivity

The real part of optical conductivity corresponding to the imaginary part of the dielectric function is shown in Fig. 10(a and b) for 1H and-1T-MgF_2 monolayer. Optical conductivity for (E||X) and (E|| Z) is zero when the energy is < 3.98 eV and 4 eV respectively confirm that of 1H-MgF_2 monolayer has semiconducting properties. The maximum optical conductivity for (E||Z) correspond to energy of 16 eV and for (E||Z) corresponds to energy of 19.68 eV. Optical conductivity for 1T-MgF_2 (E||X) and (E||Z) is zero when the energy is < 4.38 eV and 4.38 eV respectively which confirm that MgF_2 monolayer has inductor property. The maximum optical conductivity for (E||X) correspond to energy of 18.00 eV and for (E||Z) corresponds to energy of 16.22 eV.

4. Conclusion

In summary, the structural, electronic band structure, density of states and optical properties of 1H- and 1T-MgF_2 phase in 2D monolayer and bulk phase of MgF_2 have been calculated using the density functional theory (DFT). The result shows that the bulk tetragonal MgF_2, 1H- and 1T-MgF_2 monolayer are direct band gap (pure insulator) with band gap are 7.07 eV, 6.16 eV and 7.56 eV, respectively. Optical anisotropy is observed from light polarization parallel and perpendicular to 1H- and 1T MgF_2 monolayer. The dielectric function, refractive index, absorption spectrum and electron energy loss spectra are calculated using band structure and density of states. The calculated static refractive index are 1.37 (1H-phase), 1.33 (1T-phase) and 1.39 (1H-phase), 1.375 (1T-phase) for perpendicular and parallel polarization direction, respectively. This provides a theoretical basis for the design of material has promising applications in anti-reflection coatings and high-reflective systems and also application of MgF_2 monolayer in opto-electronic materials.

References

[1] M. Zukic, D.G. Torr, J.F. Spann, M.R. Torr, Appl. Opt. 29 (1990) 4284.
[2] M.L. Protopapa, F.D. Tomasi, M.R. Perrone, A. Piegari, E. Masetti, D. Ristau, J. Vac. Sci. Technol. A 19 (2001) 681.
[3] M.Q. Zhang, W.D. Gao, T.Y. Tan, H.B. He, J.D. Shao, Z.X. Fan, Vacuum 79 (2005) 90.
[4] L.G. Jacobsohn, A.L. Roy, C.L. McPherson, C.J. Kucera, L.C. Oliveria, E.G. Yukihara, Opt. Mater 35 (2013) 2461.
[5] J. Haber, M. Wojciechowska, J. Catal. 110 (1988) 23.
[6] J. Haber, M. Wojciechowska, Catal. Lett. 10 (1991) 271.
[7] S. Behzad, J. Mater. Sci. Electr. 26 (2015) 9898–9906.
[8] C.C. Lin, R.S. Liu, J. Phys. Chem. Lett. 2 (2011) 1268–1277.
[9] L.Vriens, G.Acket, C. Ronda, U.S. Patent No. 5,813,753, 1998.
[10] (a) W. Maria, M. Zieliński, M. Pietrowski, Fluor. Chem. 120.1 (2003) 1–11 (12); (b) H.R. Soni, S.K. Gupta, M. Talati, P.K. Jha, J. Phys. Chem. Solids 72 (2011) 934.
[11] A.F. Vassilyeva, R.I. Eglitis, E.A. Kotomin, A.K. Dauletbekova, Physica B 405 (2010) 2125–2127.
[12] K. Scheurell, J. Noack, R. König, J. Hegmann, R. Jahn, T. Hofmann, E. Kemnitz, Dalton Trans. 44 (2015) 19501–19508.
[13] M. Wojciechowska, W. Gut, V. Szymenderska, Catal. Lett. 7 (1990) 431.
[14] S. Ghahramani, H. Kangarlau, J. Nano, Electron. Phys. 5 (2013) 4051.
[15] M. Wojciechowska, S. Łomnicki, J. Bartoszewicz, J. Goslar, J. Chem. Soc. Faraday Trans. 91 (1995) 2207.
[16] E. Eva, K. Mann, N. Kaiser, B. Anton, R. Henking, D. Ristau, P. Weissbrodt, D. Mademann, L. Raupach, E. Hacker, Appl. Opt. 35 (1996) 5613.
[17] M. Wojciechowska, J. Haber, S. Łomnicki, J. Mol. Catal. 141 (1999) 155.
[18] M. Wojciechowska, M. Pietrowski, S. Łomnicki, B. Czajka, Catal. Lett. 46 (1997) 63.
[19] M. Wojciechowska, M. Pietrowski, S. Łomnicki, Chem. Commun. 5 (1999) 463.
[20] M. Scrocco, Phys. Rev. B 33 (1986) 7228.
[21] P. Patnaik, Handbook of Inorganic Chemicals, McGraw Hill, New York, 2002.
[22] I. Korepanov, V.M. Lisitsyn, Sov. Izv. Vuzov Fiz. 9 (1977) 146.
[23] V.M. Lisitsyn, V.I. Korepanov, V.Yu Yakovlev, Russ. Phys. J. 39 (1996) 1009.
[24] Z. Yi, J. Ran, J. Phys. Condens Mater. 24 (2012) 085602.
[25] G. Kresse, J. Furthmüller, Phys. Rev. B 54 (1996) 11169.
[26] G. Kresse, J. Furthmüller, Comp. Mater. Sci. 6 (1996) 15.
[27] G. Kresse, J. Hafner, Phys. Rev. B 47 (1993) 558.
[28] G. Kresse, D. Joubert, Phys. Rev. B 59 (1999) 1758.
[29] J.P. Perdew, K. Burke, M. Ernzerhof, Phys. Rev. Lett. 77 (1996) 3865.
[30] M. Gajdoš, K. Hummer, G. Kresse, Phys. Rev. B 73 (2006) 045112.
[31] D. Singh, S.K. Gupta, Y.A. Sonvane, I. Lukačević, J. Mater. Chem. C 4 (2016) 6386–6390.
[32] K.R. Babu, C.B. Lingam, S. Auluck, S.P. Tewari, G. Vaitheeswaran, Solid State Chem. 184 (2011) 343–350.
[33] V. Kanchana, G. Vaitheeswaran, M. Rajagopalan, Alloy Compd. 352 (2003) 60–65.
[34] L.P. Wang, Z.X. Zhang, C.L. Zhang, B.S. Xu Comp, Mater. Sci. 77 (2013) 281.
[35] A.T. Davidson, A.M.J. Raphuthi, J.D. Comins, T.E. Derry Nucl, Instrum. Methods B 80 (1993) 1237.
[36] J. Thomas, G. Stephan, J.C. Lemonnier, M. Nisar, S. Robin, Phys. Status Solidi B 56 (1973) 163.
[37] M.W. Williams, R.A. Macrae, E.T. Arakawa, J. Appl. Phys. 38 (1967) 1701.
[38] S.H. Woo, S.H. Kim, C.K. Hwangbo, J. Korean Phys. Soc. 45 (1) (2004) 99–107.
[39] A. Ziletti, S.M. Huang, D.F. Coker, H. Lin, Phys. Rev. B 92 (2015) 085423.
[40] K.R. Babu, C.B. Lingam, S. Auluck, S.P. Tewari, G. Vaitheeswaran, J. Solid State Chem. 184 (2011) 343.
[41] S. Behzad, J. Mater. Sci.-Mater. El. 26 (2015) 9898.
[42] L. Zhen-Li, A. Xin-You, C. Xin-Lu, W. Xue-Min, Z. Hong, P. Li-Ping, W. Wei-Dong, Chin. Phys. B 23 (2014) 037104.